Applications of Mathematics

Jan Zapletal; Jiří Bouchala

Effective semi-analytic integration for hypersingular Galerkin boundary integral equations for the Helmholtz equation in 3D

Applications of Mathematics, Vol. 59 (2014), No. 5, 527--542

Persistent URL: http://dml.cz/dmlcz/143929

59 (2014) APPLICATIONS OF MATHEMATICS No. 5, 527–542

EFFECTIVE SEMI-ANALYTIC INTEGRATION FOR HYPERSINGULAR GALERKIN BOUNDARY INTEGRAL EQUATIONS FOR THE HELMHOLTZ EQUATION IN 3D

Jan Zapletal, Jiří Bouchala, Ostrava

(Received January 5, 2013)

Abstract. We deal with the Galerkin discretization of the boundary integral equations corresponding to problems with the Helmholtz equation in 3D. Our main result is the semi-analytic integration for the bilinear form induced by the hypersingular operator. Such computations have already been proposed for the bilinear forms induced by the single-layer and the double-layer potential operators in the monograph *The Fast Solution of Boundary Integral Equations* by O. Steinbach and S. Rjasanow and we base our computations on these results.

Keywords: boundary element method; Galerkin discretization; Helmholtz equation; hypersingular boundary integral equation

MSC 2010: 65N38

Introduction

The boundary element method (BEM) has started to play an important role in modern mathematics during the last few decades. Together with the finite element method (FEM) it belongs to the most widely used numerical schemes for solving elliptic partial differential equations. Contrary to FEM based on the classic variational

This research has been supported by the grant of the Ministry of Education of the Czech Republic No. MSM6198910027, by VŠB-Technical University of Ostrava under the grant SGS SP2013/191, by the European Regional Development Fund in the IT4Innovations Centre of Excellence project (CZ.1.05/1.1.00/02.0070) and by the project SPOMECH-Creating a multidisciplinary R&D team for reliable solution of mechanical problems, reg. no. CZ.1.07/2.3.00/20.0070 within the Operational Programme 'Education for competitiveness' funded by the Structural Funds of the European Union and the state budget of the Czech Republic.

formulation of the given problem, the core of BEM is the boundary integral formulation leading to a dimension reduction. This approach is particularly advantageous when solving a problem on an unbounded domain that is reduced to a boundary integral equation (BIE) on a compact boundary. A typical example of such a problem is sound scattering described by the Helmholtz equation. On the other hand, one has to deal with fully populated matrices and most importantly with integration of singular functions.

One of the discretization techniques for BIEs is the Galerkin scheme comprising an additional integration of the integral equation over the boundary. Since the integrands are rather complex (and singular) functions, in 3D it seems impossible to compute both the surface integrals analytically. There exist several possibilities of setting up the Galerkin matrices. One of them is a fully numerical scheme using a transformation rendering the integrands analytic (see, e.g., [7]). However, it is also possible to compute the inner integral analytically and use a suitable quadrature scheme for the remaining one. In [6], the analytic formulae are provided for the single-layer and the double-layer potential operators. The main result of the present paper is the semi-analytic integration for the bilinear form induced by the hypersingular operator based on the above mentioned results. Moreover, the result can be used for a single-layer potential equation with the piecewise affine approximation of the Neumann data (see Remark 2.2).

1. Representation formula and BIE

We consider the exterior Neumann boundary value problem (BVP) for the Helmholtz equation

$$\text{(1.1)}\qquad \begin{cases} \Delta u + \kappa^2 u = 0 & \text{in } \Omega^{\mathrm{ext}} := \mathbb{R}^3 \setminus \overline{\Omega}, \\ \dfrac{\partial u}{\partial \boldsymbol{n}} = g_{\mathrm{N}} & \text{on } \partial\Omega, \\ \Big|\Big\langle \nabla u(\boldsymbol{x}), \dfrac{\boldsymbol{x}}{\|\boldsymbol{x}\|} \Big\rangle - \mathrm{i}\kappa u(\boldsymbol{x})\Big| = \mathcal{O}\Big(\dfrac{1}{\|\boldsymbol{x}\|^2}\Big) & \text{for } \|\boldsymbol{x}\| \to \infty, \end{cases}$$

with a bounded Lipschitz domain Ω, the wave number $\kappa \in \mathbb{R}_+$, $\boldsymbol{n}$ denoting the unit exterior normal vector to $\partial\Omega$ (note that $\boldsymbol{n}$ is directed to the exterior of Ω) and $g_{\mathrm{N}} \in H^{-1/2}(\partial\Omega)$. The Sommerfeld radiation condition ensures the uniqueness of the solution. We seek the weak solution in the Sobolev space $H^1_{\mathrm{loc}}(\Omega^{\mathrm{ext}}, \Delta)$, i.e., the space of functions in

$$H^1(\widetilde{\Omega}, \Delta) := \Big\{ u \in L^2(\widetilde{\Omega}) \colon \frac{\partial u}{\partial x_i} \in L^2(\widetilde{\Omega}) \wedge \Delta u \in L^2(\widetilde{\Omega}) \Big\}$$

for all bounded domains $\widetilde{\Omega} \subset \Omega^{\mathrm{ext}}$. The derivatives are considered in the distributional sense.

Solution to (1.1) is given by the representation formula (see [3], [6])

$$u = W_\kappa \gamma^{0,\mathrm{ext}} u - \widetilde{V}_\kappa \gamma^{1,\mathrm{ext}} u \quad \text{in } \Omega^{\mathrm{ext}} \tag{1.2}$$

with the Dirichlet and Neumann trace operators

$$\gamma^{0,\mathrm{ext}}\colon\ H^1_{\mathrm{loc}}(\Omega^{\mathrm{ext}},\Delta) \to H^{1/2}(\partial\Omega), \quad \gamma^{1,\mathrm{ext}}\colon\ H^1_{\mathrm{loc}}(\Omega^{\mathrm{ext}},\Delta) \to H^{-1/2}(\partial\Omega)$$

generalizing the concept of the restriction of a function to the boundary and the normal derivative, respectively, and the integral operators

$$\widetilde{V}_\kappa\colon\ H^{-1/2}(\partial\Omega) \to H^1_{\mathrm{loc}}(\Omega^{\mathrm{ext}},\Delta), \quad (\widetilde{V}_\kappa q)(\boldsymbol{x}) := \int_{\partial\Omega} v_\kappa(\boldsymbol{x},\boldsymbol{y}) q(\boldsymbol{y})\,\mathrm{d}\boldsymbol{s}_{\boldsymbol{y}},$$
$$W_\kappa\colon\ H^{1/2}(\partial\Omega) \to H^1_{\mathrm{loc}}(\Omega^{\mathrm{ext}},\Delta), \quad (W_\kappa t)(\boldsymbol{x}) := \int_{\partial\Omega} \frac{\partial v_\kappa}{\partial \boldsymbol{n}_{\boldsymbol{y}}}(\boldsymbol{x},\boldsymbol{y}) t(\boldsymbol{y})\,\mathrm{d}\boldsymbol{s}_{\boldsymbol{y}}.$$

The function $v_\kappa\colon\ \mathbb{R}^3 \times \mathbb{R}^3 \to \mathbb{C}$ denotes the fundamental solution for the Helmholtz equation in 3D, i.e.,

$$v_\kappa(\boldsymbol{x},\boldsymbol{y}) := \frac{1}{4\pi} \frac{\mathrm{e}^{\mathrm{i}\kappa\|\boldsymbol{x}-\boldsymbol{y}\|}}{\|\boldsymbol{x}-\boldsymbol{y}\|}.$$

To obtain the solution to (1.1) using the representation formula (1.2), we need to compute the missing Cauchy data, i.e., the missing boundary values. Since we deal with the Neumann problem (i.e., the Neumann trace $\gamma^{1,\mathrm{ext}} u = g_{\mathrm{N}}$ is given), we have to compute the Dirichlet trace $\gamma^{0,\mathrm{ext}} u$. Applying the Neumann trace operator $\gamma^{1,\mathrm{ext}}$ to (1.2) and inserting the known Neumann trace $\gamma^{1,\mathrm{ext}} u = g_{\mathrm{N}}$, we obtain the boundary integral equation defining the relation between the boundary data (see [3], [6])

$$(D_\kappa \gamma^{0,\mathrm{ext}} u)(\boldsymbol{x}) = -\frac{1}{2} g_{\mathrm{N}}(\boldsymbol{x}) - (K^*_\kappa g_{\mathrm{N}})(\boldsymbol{x}) \quad \text{for } \boldsymbol{x} \in \partial\Omega \tag{1.3}$$

with the hypersingular operator $D_\kappa\colon\ H^{1/2}(\partial\Omega) \to H^{-1/2}(\partial\Omega)$, $D_\kappa := -\gamma^{1,\mathrm{ext}} W_\kappa$, and the adjoint double-layer potential operator $K^*_\kappa\colon\ H^{-1/2}(\partial\Omega) \to H^{-1/2}(\partial\Omega)$,

$$\begin{aligned}(K^*_\kappa q)(\boldsymbol{x}) &:= \int_{\partial\Omega} \frac{\partial v_\kappa}{\partial \boldsymbol{n}_{\boldsymbol{x}}}(\boldsymbol{x},\boldsymbol{y}) q(\boldsymbol{y})\,\mathrm{d}\boldsymbol{s}_{\boldsymbol{y}} \\ &= \frac{1}{4\pi} \int_{\partial\Omega} \frac{\mathrm{e}^{\mathrm{i}\kappa\|\boldsymbol{x}-\boldsymbol{y}\|}}{\|\boldsymbol{x}-\boldsymbol{y}\|^3} (\mathrm{i}\kappa\|\boldsymbol{x}-\boldsymbol{y}\| - 1)\langle \boldsymbol{x}-\boldsymbol{y}, \boldsymbol{n}(\boldsymbol{x})\rangle q(\boldsymbol{y})\,\mathrm{d}\boldsymbol{s}_{\boldsymbol{y}} \quad \text{for } \boldsymbol{x} \in \partial\Omega.\end{aligned}$$

The boundary integral equation (1.3) is equivalent to the variational formulation

$$\int_{\partial\Omega} (D_\kappa \gamma^{0,\mathrm{ext}} u)(\boldsymbol{x}) t(\boldsymbol{x}) \,\mathrm{d}\boldsymbol{s}_{\boldsymbol{x}} = \int_{\partial\Omega} \Big(-\frac{1}{2} g_{\mathrm{N}} - K_\kappa^* g_{\mathrm{N}} \Big)(\boldsymbol{x}) t(\boldsymbol{x}) \,\mathrm{d}\boldsymbol{s}_{\boldsymbol{x}} \tag{1.4}$$

for all $t \in H^{1/2}(\partial\Omega)$. To regularize the hypersingular term on the left-hand side of (1.4), we use a representation using surface curl operators (see Theorem 3.4.2 in [4] and Theorem 3.3.22, Corollary 3.3.24 in [7]). For $q, t \in H^{1/2}(\partial\Omega)$ we have

$$\begin{aligned}\int_{\partial\Omega} (D_\kappa t)(\boldsymbol{x}) q(\boldsymbol{x}) \,\mathrm{d}\boldsymbol{s}_{\boldsymbol{x}} = {} & \frac{1}{4\pi} \int_{\partial\Omega} \int_{\partial\Omega} \frac{\mathrm{e}^{\mathrm{i}\kappa\|\boldsymbol{x}-\boldsymbol{y}\|}}{\|\boldsymbol{x}-\boldsymbol{y}\|} \langle \mathbf{curl}_{\partial\Omega}\, t(\boldsymbol{y}), \mathbf{curl}_{\partial\Omega}\, q(\boldsymbol{x}) \rangle \,\mathrm{d}\boldsymbol{s}_{\boldsymbol{y}} \,\mathrm{d}\boldsymbol{s}_{\boldsymbol{x}} \\ & - \frac{\kappa^2}{4\pi} \int_{\partial\Omega} \int_{\partial\Omega} \frac{\mathrm{e}^{\mathrm{i}\kappa\|\boldsymbol{x}-\boldsymbol{y}\|}}{\|\boldsymbol{x}-\boldsymbol{y}\|} t(\boldsymbol{y}) q(\boldsymbol{x}) \langle \boldsymbol{n}(\boldsymbol{x}), \boldsymbol{n}(\boldsymbol{y}) \rangle \,\mathrm{d}\boldsymbol{s}_{\boldsymbol{y}} \,\mathrm{d}\boldsymbol{s}_{\boldsymbol{x}}\end{aligned}$$

with the surface curl operator

$$\mathbf{curl}_{\partial\Omega}\, t(\boldsymbol{y}) := \boldsymbol{n}(\boldsymbol{y}) \times \nabla \tilde{t}(\boldsymbol{y}) \quad \text{for } \boldsymbol{y} \in \partial\Omega,$$

where $\tilde{t}$ is some locally defined extension of t into a neighbourhood of $\partial\Omega$.

In the following text we also utilize the zero-jump property of the hypersingular operator on the boundary, i.e.,

$$[\gamma^1 W_\kappa t] := \gamma^{1,\mathrm{ext}} W_\kappa t - \gamma^{1,\mathrm{int}} W_\kappa t = 0 \quad \text{for all } t \in H^{1/2}(\partial\Omega). \tag{1.5}$$

2. Numerical realization

Since the variational formula (1.4) is defined on $\partial\Omega$, we only have to discretize the boundary of $\Omega \subset \mathbb{R}^3$. To approximate $\partial\Omega$, we use a triangulation

$$\partial\Omega \approx \bigcup_{k=1}^{E} \overline{\tau_k}$$

with open triangles τ_k and assume that neighbouring elements either share a whole edge or a single vertex. We use the symbols E, N to denote the number of elements and triangulation nodes, respectively.

2.1. Galerkin equations. To approximate the given Neumann data, we use the L^2 projection into the space $T_\psi(\partial\Omega)$ of piecewise constant basis functions (see Figure 2.1a), i.e.,

$$g_{\mathrm{N}} \approx g_{\mathrm{N},h} := \arg \min_{g_\psi \in T_\psi(\partial\Omega)} \|g_{\mathrm{N}} - g_\psi\|_{L^2(\partial\Omega)} = \sum_{l=1}^{E} g_l^{\mathrm{N}} \psi_l$$

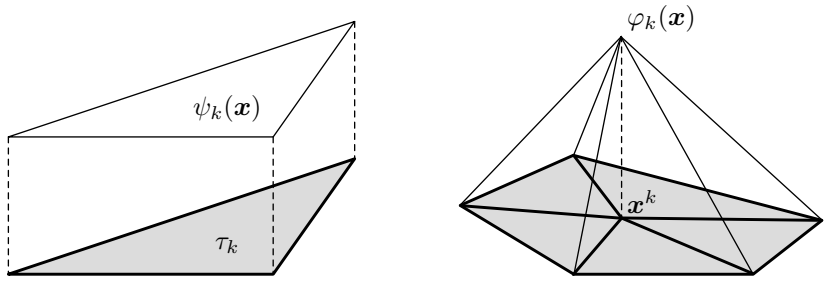

(a) Piecewise constant basis function. (b) Piecewise affine continuous basis function.

Figure 2.1. Basis functions.

and we seek the unknown Dirichlet trace in the space $T_\varphi(\partial\Omega)$ of piecewise affine continuous basis functions (see Figure 2.1b) as

$$\gamma^{0,\mathrm{ext}} u \approx g_{\mathrm{D},h} := \sum_{j=1}^{N} g_j^{\mathrm{D}} \varphi_j.$$

Inserting the approximations of the boundary data into (1.4) and choosing φ_i as the test functions, we obtain the Galerkin equations

$$\sum_{j=1}^{N} g_j^{\mathrm{D}} \int_{\partial\Omega} (D_\kappa \varphi_j)(\boldsymbol{x}) \varphi_i(\boldsymbol{x}) \,\mathrm{d}\boldsymbol{s}_{\boldsymbol{x}} = \sum_{l=1}^{E} g_l^{\mathrm{N}} \int_{\partial\Omega} \Big(-\frac{1}{2}\psi_l - K_\kappa^* \psi_l\Big)(\boldsymbol{x}) \varphi_i(\boldsymbol{x}) \,\mathrm{d}\boldsymbol{s}_{\boldsymbol{x}}$$

for $i \in \{1, \ldots, N\}$ or the matrix formulation

$$\mathsf{D}_{\kappa,h}\, \boldsymbol{g}^{\mathrm{D}} = \Big(-\frac{1}{2}\mathsf{M}_h^{\mathsf{T}} - \mathsf{K}_{\kappa,h}^{\mathsf{T}}\Big)\boldsymbol{g}^{\mathrm{N}} \tag{2.1}$$

with the vectors $\boldsymbol{g}^{\mathrm{D}} := [g_1^{\mathrm{D}}, \ldots, g_N^{\mathrm{D}}]^{\mathsf{T}}$, $\boldsymbol{g}^{\mathrm{N}} := [g_1^{\mathrm{N}}, \ldots, g_E^{\mathrm{N}}]^{\mathsf{T}}$ and the matrices $\mathsf{D}_{\kappa,h} \in \mathbb{C}^{N\times N}$, $\mathsf{M}_h \in \mathbb{R}^{E\times N}$, and $\mathsf{K}_{\kappa,h} \in \mathbb{C}^{E\times N}$ given by

$$\begin{aligned} \mathsf{D}_{\kappa,h}[i,j] &:= \frac{1}{4\pi}\int_{\partial\Omega}\int_{\partial\Omega} \frac{\mathrm{e}^{\mathrm{i}\kappa\|\boldsymbol{x}-\boldsymbol{y}\|}}{\|\boldsymbol{x}-\boldsymbol{y}\|} \langle \mathbf{curl}_{\partial\Omega}\, \varphi_j(\boldsymbol{y}), \mathbf{curl}_{\partial\Omega}\, \varphi_i(\boldsymbol{x})\rangle \,\mathrm{d}\boldsymbol{s}_{\boldsymbol{y}} \,\mathrm{d}\boldsymbol{s}_{\boldsymbol{x}} \\ &\quad - \frac{\kappa^2}{4\pi}\int_{\partial\Omega}\int_{\partial\Omega} \frac{\mathrm{e}^{\mathrm{i}\kappa\|\boldsymbol{x}-\boldsymbol{y}\|}}{\|\boldsymbol{x}-\boldsymbol{y}\|} \varphi_j(\boldsymbol{y})\varphi_i(\boldsymbol{x}) \langle \boldsymbol{n}(\boldsymbol{x}), \boldsymbol{n}(\boldsymbol{y})\rangle \,\mathrm{d}\boldsymbol{s}_{\boldsymbol{y}} \,\mathrm{d}\boldsymbol{s}_{\boldsymbol{x}}, \end{aligned} \tag{2.2}$$

$$\mathsf{M}_h[l,i] := \int_{\tau_l} \varphi_i(\boldsymbol{x}) \,\mathrm{d}\boldsymbol{s}_{\boldsymbol{x}},$$

$$\mathsf{K}_{\kappa,h}[l,i] := \frac{1}{4\pi}\int_{\tau_l}\int_{\partial\Omega} \varphi_i(\boldsymbol{y}) \frac{\mathrm{e}^{\mathrm{i}\kappa\|\boldsymbol{x}-\boldsymbol{y}\|}}{\|\boldsymbol{x}-\boldsymbol{y}\|^3}(1-\mathrm{i}\kappa\|\boldsymbol{x}-\boldsymbol{y}\|)\langle \boldsymbol{x}-\boldsymbol{y}, \boldsymbol{n}(\boldsymbol{y})\rangle \,\mathrm{d}\boldsymbol{s}_{\boldsymbol{y}} \,\mathrm{d}\boldsymbol{s}_{\boldsymbol{x}}. \tag{2.3}$$

2.2. Integration over boundary elements. To assemble the system of linear equations (2.1), it is necessary to evaluate the double surface integrals building the

matrices $\mathsf{K}_{\kappa,h}, \mathsf{D}_{\kappa,h}$. The entries in the double-layer potential matrix $\mathsf{K}_{\kappa,h}$ from (2.3) can be rewritten as

$$\begin{aligned}\mathsf{K}_{\kappa,h}[l,i] &= \frac{1}{4\pi}\int_{\tau_l}\int_{\partial\Omega}\varphi_i(\boldsymbol{y})\frac{\langle \boldsymbol{x}-\boldsymbol{y},\boldsymbol{n}(\boldsymbol{y})\rangle}{\|\boldsymbol{x}-\boldsymbol{y}\|^3}\,\mathrm{d}\boldsymbol{s}_{\boldsymbol{y}}\,\mathrm{d}\boldsymbol{s}_{\boldsymbol{x}}\\ &\quad+\frac{1}{4\pi}\int_{\tau_l}\int_{\partial\Omega}\varphi_i(\boldsymbol{y})\frac{\langle \boldsymbol{x}-\boldsymbol{y},\boldsymbol{n}(\boldsymbol{y})\rangle}{\|\boldsymbol{x}-\boldsymbol{y}\|^3}(\mathrm{e}^{\mathrm{i}\kappa\|\boldsymbol{x}-\boldsymbol{y}\|}(1-\mathrm{i}\kappa\|\boldsymbol{x}-\boldsymbol{y}\|)-1)\,\mathrm{d}\boldsymbol{s}_{\boldsymbol{y}}\,\mathrm{d}\boldsymbol{s}_{\boldsymbol{x}}.\end{aligned}$$

Since the latter integrand has no singularity for $\boldsymbol{x}\to\boldsymbol{y}$, we can use a suitable numerical quadrature for both surface integrals. In Section 3 we use the 7-point Gauss integration scheme as proposed in [6]. For the singular part corresponding to the Laplace equation (i.e., the Helmholtz equation with $\kappa=0$) we use the combination of a numerical quadrature and an analytic formula for the inner integral (see [6], Section C.2).

The first double surface integral corresponding to the hypersingular operator matrix (2.2) reads

$$\begin{aligned}\mathsf{D}^1_{\kappa,h}[i,j] &:= \frac{1}{4\pi}\int_{\partial\Omega}\int_{\partial\Omega}\frac{\mathrm{e}^{\mathrm{i}\kappa\|\boldsymbol{x}-\boldsymbol{y}\|}}{\|\boldsymbol{x}-\boldsymbol{y}\|}\langle\mathbf{curl}_{\partial\Omega}\,\varphi_j(\boldsymbol{y}),\mathbf{curl}_{\partial\Omega}\,\varphi_i(\boldsymbol{x})\rangle\,\mathrm{d}\boldsymbol{s}_{\boldsymbol{y}}\,\mathrm{d}\boldsymbol{s}_{\boldsymbol{x}}\\ &= \sum_{\tau_k\subset\operatorname{supp}\varphi_i}\sum_{\tau_l\subset\operatorname{supp}\varphi_j}\langle\mathbf{curl}_{\partial\Omega}\,\varphi_j|_{\tau_l}(\boldsymbol{y}),\mathbf{curl}_{\partial\Omega}\,\varphi_i|_{\tau_k}(\boldsymbol{x})\rangle\mathsf{V}_{\kappa,h}[k,l],\end{aligned}$$

where

$$\mathsf{V}_{\kappa,h}[k,l] := \frac{1}{4\pi}\int_{\tau_k}\int_{\tau_l}\frac{\mathrm{e}^{\mathrm{i}\kappa\|\boldsymbol{x}-\boldsymbol{y}\|}}{\|\boldsymbol{x}-\boldsymbol{y}\|}\,\mathrm{d}\boldsymbol{s}_{\boldsymbol{y}}\,\mathrm{d}\boldsymbol{s}_{\boldsymbol{x}}$$

denotes the matrix corresponding to the single-layer potential operator $V_\kappa := \gamma^{0,\mathrm{ext}}\widetilde{V}_\kappa$. These entries can be computed in the same way as in the case of the double-layer potential matrix using the combination of a numerical quadrature and an analytic formula as described in [6]. The remaining part of $\mathsf{D}_{\kappa,h}[i,j]$ can be split into

$$\begin{aligned}\mathsf{D}^2_{\kappa,h}[i,j] &= \frac{\kappa^2}{4\pi}\int_{\partial\Omega}\varphi_i(\boldsymbol{x})\int_{\partial\Omega}\frac{1}{\|\boldsymbol{x}-\boldsymbol{y}\|}\varphi_j(\boldsymbol{y})\langle\boldsymbol{n}(\boldsymbol{x}),\boldsymbol{n}(\boldsymbol{y})\rangle\,\mathrm{d}\boldsymbol{s}_{\boldsymbol{y}}\,\mathrm{d}\boldsymbol{s}_{\boldsymbol{x}}\\ &\quad+\frac{\kappa^2}{4\pi}\int_{\partial\Omega}\varphi_i(\boldsymbol{x})\int_{\partial\Omega}\frac{\mathrm{e}^{\mathrm{i}\kappa\|\boldsymbol{x}-\boldsymbol{y}\|}-1}{\|\boldsymbol{x}-\boldsymbol{y}\|}\varphi_j(\boldsymbol{y})\langle\boldsymbol{n}(\boldsymbol{x}),\boldsymbol{n}(\boldsymbol{y})\rangle\,\mathrm{d}\boldsymbol{s}_{\boldsymbol{y}}\,\mathrm{d}\boldsymbol{s}_{\boldsymbol{x}}.\end{aligned}\tag{2.4}$$

Again, the latter integrand has no singularity for $\boldsymbol{x}\to\boldsymbol{y}$ and the 7-point quadrature can be used.

R e m a r k 2.1. There exist concerns whether the Galerkin method with the semi-analytic evaluation of the matrix entries has the correct convergence order (compared to the Gakerkin method without quadrature). The authors are not aware of relevant

results in this area except for [1] and [2], where the situation is analyzed for the screen problem in $\mathbb{R}^3$ for the single-layer potential integral equation

$$(V_0 u)(\boldsymbol{x}) := \frac{1}{4\pi} \int_{\partial\Omega} \frac{1}{\|\boldsymbol{x} - \boldsymbol{y}\|} u(\boldsymbol{y}) \, \mathrm{d}\boldsymbol{s}_{\boldsymbol{y}} = f(\boldsymbol{x}) \quad \text{for all } \boldsymbol{x} \in \partial\Omega \tag{2.5}$$

with rectangular and triangular elements, respectively, and piecewise constant approximation of u. Note that the kernel function in (2.5) is exactly the same as in the singular part of (2.4) (the inner product of normal vectors is constant on each element). To show that the Galerkin scheme preserves the correct order, a subdivision of elements and a composite of a simple quadrature rule (e.g., the midpoint formula for each subelement) is used. Although our approach uses a different quadrature technique and piecewise affine basis functions, it is widely used by the BEM community as an alternative to the fully numerical evaluation methods. Moreover, the numerical results in, e.g., [5], [6] and others exhibit the correct order of convergence not only for the computed Cauchy data, but also for the pointwise evaluation in the computational domain.

R e m a r k 2.2. Our result is also useful for the evaluation of the Laplace part of the single-layer potential matrix with the piecewise affine approximation of the density function (the Neumann data in our case). Moreover, if one uses the collocation scheme instead of the Galerkin approach, it is necessary to evaluate the entries given by

$$\widehat{\mathrm{V}}_{0,h}[i,j] := \frac{1}{4\pi} \int_{\partial\Omega} \frac{1}{\|\boldsymbol{x}_i - \boldsymbol{y}\|} \varphi_j(\boldsymbol{y}) \, \mathrm{d}\boldsymbol{s}_{\boldsymbol{y}}$$

for every collocation point $\boldsymbol{x}_i$. Note that the surface integral is exactly the one we consider in this paper. In this way, the numerical integration is completely avoided, but one ends up with nonsymmetric system matrices.

To compute the inner integral of the singular part in (2.4), we use the local coordinate system $\boldsymbol{r}^1, \boldsymbol{r}^2, \boldsymbol{n}$ corresponding to a general triangular element τ with nodes $\boldsymbol{x}^1, \boldsymbol{x}^2, \boldsymbol{x}^3$ as introduced in [6] (see Figure 2.2a).

We define the vector $\boldsymbol{r}^2$ as

$$\boldsymbol{r}^2 := \frac{1}{t_\tau}(\boldsymbol{x}^3 - \boldsymbol{x}^2),$$

where t_τ denotes the length of the side $\overline{\boldsymbol{x}^2\boldsymbol{x}^3}$, i.e., $t_\tau := \|\boldsymbol{x}^3 - \boldsymbol{x}^2\|$. We introduce an auxiliary point $\boldsymbol{x}^*$ lying on the intersection of the line defined by the side $\overline{\boldsymbol{x}^2\boldsymbol{x}^3}$ and the altitude coming through $\boldsymbol{x}^1$. Thus, we can write

$$\boldsymbol{x}^* := \boldsymbol{x}^2 + t_* \boldsymbol{r}^2 \quad \text{with } t_* := \langle \boldsymbol{x}^1 - \boldsymbol{x}^2, \boldsymbol{r}^2 \rangle.$$

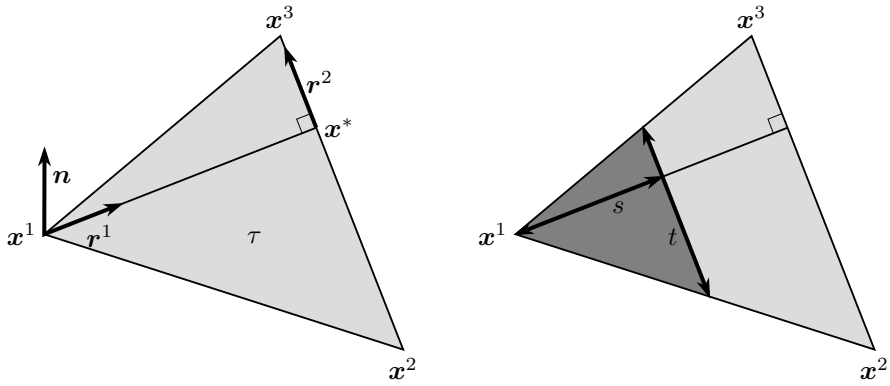

(a) Local coordinate system corresponding to τ. (b) Triangle parametrization.

Figure 2.2. Analytic integration over triangles.

Then we define

$$\boldsymbol{r}^1 := \frac{1}{s_\tau}(\boldsymbol{x}^* - \boldsymbol{x}^1) \quad \text{with } s_\tau := \|\boldsymbol{x}^* - \boldsymbol{x}^1\|.$$

The last coordinate vector orthogonal to both $\boldsymbol{r}^1$ and $\boldsymbol{r}^2$ is defined as

$$\boldsymbol{n} := \boldsymbol{r}^1 \times \boldsymbol{r}^2 = \frac{(\boldsymbol{x}^2 - \boldsymbol{x}^1) \times (\boldsymbol{x}^3 - \boldsymbol{x}^2)}{\|(\boldsymbol{x}^2 - \boldsymbol{x}^1) \times (\boldsymbol{x}^3 - \boldsymbol{x}^2)\|}.$$

Any point $\boldsymbol{x} \in \mathbb{R}^3$ can now be expressed as $\boldsymbol{x} = \boldsymbol{x}^1 + s_{\boldsymbol{x}}\boldsymbol{r}^1 + t_{\boldsymbol{x}}\boldsymbol{r}^2 + u_{\boldsymbol{x}}\boldsymbol{n}$, where

$$s_{\boldsymbol{x}} := \langle \boldsymbol{x} - \boldsymbol{x}^1, \boldsymbol{r}^1 \rangle, \quad t_{\boldsymbol{x}} := \langle \boldsymbol{x} - \boldsymbol{x}^1, \boldsymbol{r}^2 \rangle, \quad u_{\boldsymbol{x}} := \langle \boldsymbol{x} - \boldsymbol{x}^1, \boldsymbol{n} \rangle.$$

To derive the parametrization of the triangle, we introduce two more quantities, namely the tangents of the angles between the altitude $\overline{\boldsymbol{x}^1\boldsymbol{x}^*}$ and the sides $\overline{\boldsymbol{x}^1\boldsymbol{x}^2}$ and $\overline{\boldsymbol{x}^1\boldsymbol{x}^3}$, respectively. These values can be expressed as

$$\alpha_1 := -\frac{t_*}{s_\tau}, \quad \alpha_2 := \frac{t_\tau - t_*}{s_\tau}.$$

Using these parameters together with s_τ, we can parametrize the triangle τ as

$$\tau = \{\boldsymbol{y} = \boldsymbol{y}(s,t) = \boldsymbol{x}^1 + s\boldsymbol{r}^1 + t\boldsymbol{r}^2 \colon\ 0 < s < s_\tau,\ \alpha_1 s < t < \alpha_2 s\}.$$

See Figure 2.2b for the illustration of the parametrization. For any point $\boldsymbol{x} \in \mathbb{R}^3$ and a point $\boldsymbol{y} \in \tau$ we have

$$\|\boldsymbol{x} - \boldsymbol{y}\|^2 = \|(s_{\boldsymbol{x}} - s)\boldsymbol{r}^1 + (t_{\boldsymbol{x}} - t)\boldsymbol{r}^2 + u_{\boldsymbol{x}}\boldsymbol{n}\|^2 = (s - s_{\boldsymbol{x}})^2 + (t - t_{\boldsymbol{x}})^2 + u_{\boldsymbol{x}}^2.$$

To compute the local element contributions for the singular part of (2.4), we have to evaluate

$$
\begin{aligned}
(2.6)\quad S_D(\tau,\boldsymbol{x}) &:= \frac{\kappa^2}{4\pi}\int_\tau \varphi_1(\boldsymbol{y})\frac{1}{\|\boldsymbol{x}-\boldsymbol{y}\|}\,\mathrm{d}\boldsymbol{s}_{\boldsymbol{y}} \\
&= \frac{\kappa^2}{4\pi}\int_0^{s_\tau}\frac{s_\tau - s}{s_\tau}\int_{\alpha_1 s}^{\alpha_2 s}\frac{1}{\sqrt{(s-s_{\boldsymbol{x}})^2+(t-t_{\boldsymbol{x}})^2+u_{\boldsymbol{x}}^2}}\,\mathrm{d}t\,\mathrm{d}s \\
&= \frac{\kappa^2}{4\pi}\int_0^{s_\tau}\Big(1-\frac{s}{s_\tau}\Big)\big[\ln(t-t_{\boldsymbol{x}}+\sqrt{(s-s_{\boldsymbol{x}})^2+(t-t_{\boldsymbol{x}})^2+u_{\boldsymbol{x}}^2})\big]_{\alpha_1 s}^{\alpha_2 s}\,\mathrm{d}s
\end{aligned}
$$

with the affine function φ_1 defined on τ as $\varphi_1(\boldsymbol{x}^1) := 1$, $\varphi_1(\boldsymbol{x}^2) := 0$, $\varphi_1(\boldsymbol{x}^3) := 0$. Note that to compute the integral with the remaining basis functions it is sufficient to rotate the triangle. The last integral in (2.6) is similar to the integral corresponding to the single-layer potential in ([6], p. 246). Using this result, we can write

$$
S_D(\tau,\boldsymbol{x}) = \frac{\kappa^2}{4\pi}(F_D(s_\tau,\alpha_2) - F_D(0,\alpha_2) - F_D(s_\tau,\alpha_1) + F_D(0,\alpha_1)),
$$

where

$$
F_D(s,\alpha) := F_V(s,\alpha)\Big(1-\frac{p+s_{\boldsymbol{x}}}{2s_\tau}\Big) - \frac{1}{s_\tau}I_1
$$

with

$$
\begin{aligned}
(2.7)\quad F_V(s,\alpha) &:= (s-s_{\boldsymbol{x}})\ln(\alpha s - t_{\boldsymbol{x}} + \sqrt{(s-s_{\boldsymbol{x}})^2+(\alpha s-t_{\boldsymbol{x}})^2+u_{\boldsymbol{x}}^2}) - s \\
&+ \frac{\alpha s_{\boldsymbol{x}} - t_{\boldsymbol{x}}}{\sqrt{1+\alpha^2}}\ln(\sqrt{1+\alpha^2}(s-p) + \sqrt{(s-s_{\boldsymbol{x}})^2+(\alpha s-t_{\boldsymbol{x}})^2+u_{\boldsymbol{x}}^2}) \\
&+ 2u_{\boldsymbol{x}}\arctan\frac{(q-\frac{\alpha s_{\boldsymbol{x}}-t_{\boldsymbol{x}}}{1+\alpha^2})\sqrt{(s-s_{\boldsymbol{x}})^2+(\alpha s-t_{\boldsymbol{x}})^2+u_{\boldsymbol{x}}^2} + (\alpha s - t_{\boldsymbol{x}} - q)q}{(s-p)u_{\boldsymbol{x}}},
\end{aligned}
$$

parameters

$$
p := \frac{\alpha t_{\boldsymbol{x}} + s_{\boldsymbol{x}}}{1+\alpha^2}, \qquad q := \sqrt{u_{\boldsymbol{x}}^2 + \frac{(t_{\boldsymbol{x}} - \alpha s_{\boldsymbol{x}})^2}{1+\alpha^2}}
$$

and the integral

$$
I_1 := \int\Big(s - \frac{p+s_{\boldsymbol{x}}}{2}\Big)\ln\big(\alpha s - t_{\boldsymbol{x}} + \sqrt{(1+\alpha^2)(s-p)^2+q^2}\big)\,\mathrm{d}s.
$$

The possible singularities in (2.7) need to be discussed. Although the arguments of the logarithms are non-negative, they may vanish. However, in both cases the situation is similar to $\lim\limits_{x\to 0_+} x\ln x$. In the case of $u_x = 0$, i.e., the point $\boldsymbol{x}$ lying in the plane defined by the triangle τ, we can set the arctangent part equal to zero due

to the jump property of V_κ (similar to (1.5)) and the boundedness of the arctangent function. Finally, in the case when $s = p$, the last part of the function F_V becomes

$$2u_{\boldsymbol{x}} \arctan \frac{\alpha q}{u_{\boldsymbol{x}}}.$$

For the integral I_1 we use per partes with

$$\begin{aligned}
u &= \ln(\alpha s - t_{\boldsymbol{x}} + \sqrt{(1+\alpha^2)(s-p)^2 + q^2}),\\
u' &= \frac{\alpha\sqrt{(1+\alpha^2)(s-p)^2+q^2} + (1+\alpha^2)(s-p)}{(\alpha s - t_{\boldsymbol{x}})\sqrt{(1+\alpha^2)(s-p)^2+q^2} + (1+\alpha^2)(s-p)^2 + q^2},\\
v' &= s - \frac{p + s_{\boldsymbol{x}}}{2},\\
v &= \frac{1}{2}(s-p)(s-s_{\boldsymbol{x}})
\end{aligned}$$

to obtain

$$I_1 = \frac{1}{2}(s-p)(s-s_{\boldsymbol{x}}) \ln\bigl(\alpha s - t_{\boldsymbol{x}} + \sqrt{(1+\alpha^2)(s-p)^2+q^2}\bigr) - \frac{1}{2} I_2$$

with

$$\begin{aligned}
I_2 &:= \int (s-p)(s-s_{\boldsymbol{x}}) \frac{\alpha\sqrt{(1+\alpha^2)(s-p)^2+q^2} + (1+\alpha^2)(s-p)}{(\alpha s - t_{\boldsymbol{x}})\sqrt{(1+\alpha^2)(s-p)^2+q^2} + (1+\alpha^2)(s-p)^2 + q^2} \,\mathrm{d}s\\
&= \frac{s^2}{2} - ps + I_3,
\end{aligned}$$

where

$$I_3 := \int (s-p) \frac{(t_{\boldsymbol{x}} - \alpha s_{\boldsymbol{x}})\sqrt{(1+\alpha^2)(s-p)^2+q^2} + (1+\alpha^2)(s-p)(p-s_{\boldsymbol{x}}) - q^2}{(1+\alpha^2)(s-p)^2 + q^2 + (\alpha s - t_{\boldsymbol{x}})\sqrt{(1+\alpha^2)(s-p)^2+q^2}} \,\mathrm{d}s.$$

With the substitution

$$s = p + \frac{q}{\sqrt{1+\alpha^2}} \sinh u, \qquad \frac{\mathrm{d}s}{\mathrm{d}u} = \frac{q}{\sqrt{1+\alpha^2}} \cosh u$$

proposed in ([6], page 247), we obtain

$$\begin{aligned}
I_3 = {} & \frac{q^2}{\sqrt{1+\alpha^2}}\\
& \times \int \sinh u \frac{\sqrt{1+\alpha^2}(t_{\boldsymbol{x}} - \alpha s_{\boldsymbol{x}}) \cosh u + \alpha(t_{\boldsymbol{x}} - \alpha s_{\boldsymbol{x}}) \sinh u - q\sqrt{1+\alpha^2}}{q(1+\alpha^2)\cosh u + \alpha q\sqrt{1+\alpha^2}\sinh u + \alpha s_{\boldsymbol{x}} - t_{\boldsymbol{x}}} \,\mathrm{d}u.
\end{aligned}$$

With another substitution from [6]

$$v = \tanh\frac{u}{2}, \quad \sinh u = \frac{2v}{1-v^2}, \quad \cosh u = \frac{1+v^2}{1-v^2}, \quad \frac{\mathrm{d}u}{\mathrm{d}v} = \frac{2}{1-v^2}$$

we have

$$I_3 = \frac{4q^2}{\sqrt{1+\alpha^2}} \int \frac{v}{1-v^2} \frac{1}{1-v^2} \frac{B_2v^2+B_1v+B_0}{A_2v^2+A_1v+A_0}\,\mathrm{d}v$$

with the parameters

$$\begin{aligned} B_2 &:= \sqrt{1+\alpha^2}(t_{\boldsymbol{x}} - \alpha s_{\boldsymbol{x}} + q), & A_2 &:= (1+\alpha^2)q - (\alpha s_{\boldsymbol{x}} - t_{\boldsymbol{x}}),\\ B_1 &:= 2\alpha(t_{\boldsymbol{x}} - \alpha s_{\boldsymbol{x}}), & A_1 &:= 2\alpha q\sqrt{1+\alpha^2},\\ B_0 &:= \sqrt{1+\alpha^2}(t_{\boldsymbol{x}} - \alpha s_{\boldsymbol{x}} - q), & A_0 &:= (1+\alpha^2)q + (\alpha s_{\boldsymbol{x}} - t_{\boldsymbol{x}}). \end{aligned}$$

For the decomposition of the fractions in I_3 we get (see [6], pages 247–248)

$$\frac{4q^2}{\sqrt{1+\alpha^2}} \frac{v}{1-v^2} \frac{1}{1-v^2} \frac{B_2v^2+B_1v+B_0}{A_2v^2+A_1v+A_0} = \frac{v}{1-v^2}\Big(\frac{C_1}{1-v^2} + \frac{C_2}{A_2v^2+A_1v+A_0}\Big)$$

with

$$C_1 := \frac{4q(t_{\boldsymbol{x}} - \alpha s_{\boldsymbol{x}})}{1+\alpha^2}, \qquad C_2 := -4qu_{\boldsymbol{x}}^2.$$

Hence,

$$I_3 = \frac{2q(t_{\boldsymbol{x}} - \alpha s_{\boldsymbol{x}})}{1+\alpha^2} \frac{1}{1-v^2} - 4qu_{\boldsymbol{x}}^2 \int \frac{v}{1-v^2} \frac{1}{A_2v^2+A_1v+A_0}\,\mathrm{d}v.$$

The fractions from the remaining integral can be decomposed as

$$4qu_{\boldsymbol{x}}^2 \frac{v}{1-v^2} \frac{1}{A_2v^2+A_1v+A_0} = \frac{D_1}{1-v} + \frac{D_2}{1+v} + \frac{D_3v+D_4}{A_2v^2+A_1v+A_0}$$

with the coefficients

$$\begin{aligned} D_1 &:= \frac{1}{\sqrt{1+\alpha^2}} \frac{u_{\boldsymbol{x}}^2}{\sqrt{1+\alpha^2}+\alpha}, & D_3 &:= (D_1 - D_2)A_2 = 2u_{\boldsymbol{x}}^2 A_2,\\ D_2 &:= -\frac{1}{\sqrt{1+\alpha^2}} \frac{u_{\boldsymbol{x}}^2}{\sqrt{1+\alpha^2}-\alpha}, & D_4 &:= -(D_1 + D_2)A_0 = \frac{2u_{\boldsymbol{x}}^2 \alpha A_0}{\sqrt{1+\alpha^2}}. \end{aligned}$$

Thus, for I_3 we have

$$\begin{aligned} I_3 = {} & \frac{2q(t_{\boldsymbol{x}} - \alpha s_{\boldsymbol{x}})}{1+\alpha^2} \frac{1}{1-v^2} + \frac{1}{\sqrt{1+\alpha^2}} \frac{u_{\boldsymbol{x}}^2}{\sqrt{1+\alpha^2}+\alpha} \ln|1-v| \\ & + \frac{1}{\sqrt{1+\alpha^2}} \frac{u_{\boldsymbol{x}}^2}{\sqrt{1+\alpha^2}-\alpha} \ln|1+v| - u_{\boldsymbol{x}}^2 \ln|A_2v^2+A_1v+A_0| \\ & - \frac{2\alpha u_{\boldsymbol{x}}(\alpha s_{\boldsymbol{x}} - t_{\boldsymbol{x}})}{1+\alpha^2} \arctan\frac{2A_2v+A_1}{2u_{\boldsymbol{x}}\sqrt{1+\alpha^2}}. \end{aligned}$$

Collecting all terms together, we finally obtain

$$\begin{aligned}
F_D(s,\alpha) = F_V(s,\alpha)\Big(1-\frac{p+s_{\boldsymbol{x}}}{2s_\tau}\Big)\\
&-\frac{1}{2s_\tau}\bigg[(s-p)(s-s_{\boldsymbol{x}})\ln\big(\alpha s - t_{\boldsymbol{x}} + \sqrt{(1+\alpha^2)(s-p)^2+q^2}\big) - \frac{s^2}{2} + ps\\
&-\frac{2q(t_{\boldsymbol{x}}-\alpha s_{\boldsymbol{x}})}{1+\alpha^2}\frac{1}{1-v^2} - \frac{1}{\sqrt{1+\alpha^2}}\frac{u_{\boldsymbol{x}}^2}{\sqrt{1+\alpha^2}+\alpha}\ln|1-v|\\
&-\frac{1}{\sqrt{1+\alpha^2}}\frac{u_{\boldsymbol{x}}^2}{\sqrt{1+\alpha^2}-\alpha}\ln|1+v| + u_{\boldsymbol{x}}^2\ln|A_2v^2+A_1v+A_0|\\
&+\frac{2\alpha u_{\boldsymbol{x}}(\alpha s_{\boldsymbol{x}}-t_{\boldsymbol{x}})}{1+\alpha^2}\arctan\frac{2A_2v+A_1}{2u_{\boldsymbol{x}}\sqrt{1+\alpha^2}}\bigg].
\end{aligned}$$

Note that the previous formula can be directly evaluated for $u_{\boldsymbol{x}} \neq 0$ corresponding to the case when $\boldsymbol{x}$ does not lie in the plane defined by τ. In the case of $u_{\boldsymbol{x}} = 0$ the jump property of the hypersingular operator (1.5) allows us to take the limit $u_{\boldsymbol{x}} \to 0$. The terms with singularity for $v = \pm 1$ all vanish for $u_{\boldsymbol{x}} \to 0$ and it only remains to treat the term $u_{\boldsymbol{x}}^2 \ln|A_2v^2 + A_1v + A_0|$. For the discriminant of $A_2v^2 + A_1v + A_0$ we have

$$A_1^2 - 4A_2A_0 = -4(1+\alpha^2)u_{\boldsymbol{x}}^2$$

and thus the polynomial only has a real root for $u_{\boldsymbol{x}} = 0$. For $u_{\boldsymbol{x}} \neq 0$ we have $A_2 \neq 0$ and

$$\begin{aligned}
|u_{\boldsymbol{x}}^2 \ln|A_2v^2+A_1v+A_0|| &\leqslant |u_{\boldsymbol{x}}^2 \ln|A_2v_0^2+A_1v_0+A_0||\\
&= \bigg|u_{\boldsymbol{x}}^2 \ln\Big|\frac{(1+\alpha^2)q^2-(\alpha s_{\boldsymbol{x}}-t_{\boldsymbol{x}})^2}{(1+\alpha^2)q-(\alpha s_{\boldsymbol{x}}-t_{\boldsymbol{x}})}\Big|\bigg|
\end{aligned}$$

with

$$v_0 := -\frac{A_1}{2A_2} = -\frac{\alpha q\sqrt{1+\alpha^2}}{(1+\alpha^2)q-(\alpha s_{\boldsymbol{x}}-t_{\boldsymbol{x}})}$$

corresponding to the vertex of the parabola. In the case of $\alpha s_{\boldsymbol{x}} = t_{\boldsymbol{x}}$ we have

$$K := \frac{(1+\alpha^2)q^2-(\alpha s_{\boldsymbol{x}}-t_{\boldsymbol{x}})^2}{(1+\alpha^2)q-(\alpha s_{\boldsymbol{x}}-t_{\boldsymbol{x}})} = |u_{\boldsymbol{x}}|$$

and for the limit we get

$$\lim_{u_{\boldsymbol{x}}\to 0}\big|u_{\boldsymbol{x}}^2 \ln|u_{\boldsymbol{x}}|\big| = 0.$$

Now we consider the situation $\alpha s_{\boldsymbol{x}} \neq t_{\boldsymbol{x}}$ and $\alpha \neq 0$. For K we have

$$K = u_{\boldsymbol{x}}^2\frac{(1+\alpha^2)}{(1+\alpha^2)\sqrt{u_{\boldsymbol{x}}^2+(\alpha s_{\boldsymbol{x}}-t_{\boldsymbol{x}})^2/(1+\alpha^2)}-(\alpha s_{\boldsymbol{x}}-t_{\boldsymbol{x}})}$$

with a nonzero limit of the denominator. Thus, the function $\left|u_{\boldsymbol{x}}^2 \ln|K|\right|$ behaves like

$$\left|u_{\boldsymbol{x}}^2 \ln|cu_{\boldsymbol{x}}^2|\right| \to 0 \quad \text{for } u_{\boldsymbol{x}} \to 0. \tag{2.8}$$

Finally, let us assume the case of $\alpha s_{\boldsymbol{x}} \neq t_{\boldsymbol{x}}$ and $\alpha = 0$. For K we have

$$K = \frac{u_{\boldsymbol{x}}^2}{\sqrt{u_{\boldsymbol{x}}^2 + t_{\boldsymbol{x}}^2} + t_{\boldsymbol{x}}}.$$

For $t_{\boldsymbol{x}} \geqslant 0$ the limit is similar to (2.8). For $t_{\boldsymbol{x}} < 0$ we have

$$K = \frac{u_{\boldsymbol{x}}^2}{\sqrt{u_{\boldsymbol{x}}^2 + t_{\boldsymbol{x}}^2} + t_{\boldsymbol{x}}} \frac{\sqrt{u_{\boldsymbol{x}}^2 + t_{\boldsymbol{x}}^2} - t_{\boldsymbol{x}}}{\sqrt{u_{\boldsymbol{x}}^2 + t_{\boldsymbol{x}}^2} - t_{\boldsymbol{x}}} = \sqrt{u_{\boldsymbol{x}}^2 + t_{\boldsymbol{x}}^2} - t_{\boldsymbol{x}}$$

and the term $\left|u_{\boldsymbol{x}}^2 \ln|K|\right|$ vanishes for $u_{\boldsymbol{x}} \to 0$.

3. Numerical experiments

In the last section we provide numerical solutions to several exterior Neumann boundary value problems using BEM as described above. Let us first consider the problem (1.1) with $\kappa \in \{2.0, 4.0\}$, Ω being an open unit ball and the testing solution $u(\boldsymbol{x}) := v_\kappa(\boldsymbol{x}, \boldsymbol{y}_1)$ with $\boldsymbol{y}_1 := [0.9, 0.0, 0.0]^\mathsf{T}$. For the discretization of the domain we use the unit icosahedron, whose nodes are mapped to the sphere after each refinement step. In this way, an almost uniform mesh is constructed.

To compute the missing Dirichlet data, we use the system of linear equations (2.1). The approximate solution inside the domain can be computed using a discretized version of the representation formula (1.2). The results are summarized in Tables 3.1, 3.2 for $\kappa = 2.0$ and $\kappa = 4.0$, respectively. The first three columns correspond to the mesh properties, namely to the number of elements and nodes, and the mesh parameter $h := \max \sqrt{\Delta_\tau}$, with Δ_τ denoting the surface area of the triangular element τ. For the first discretization with 80 elements (the icosahedron after one refinement step) we have $h_{\text{ref}} = 4.07 \cdot 10^{-1}$, the parameter halves with every refinement step. In the subsequent columns we provide the L^2 relative errors given by

$$\text{Err}_{\text{D}} := \frac{\|g_{\text{D}} - g_{\text{D},h}\|_{L^2(\partial\Omega)}}{\|g_{\text{D}}\|_{L^2(\partial\Omega)}}, \quad \text{Err}_{\text{D},p} := \frac{\|g_{\text{D}} - g_{\text{D},p}\|_{L^2(\partial\Omega)}}{\|g_{\text{D}}\|_{L^2(\partial\Omega)}},$$

with g_{D}, $g_{\text{D},h}$, $g_{\text{D},p}$ denoting the exact, computed and L^2 projected exact Dirichlet data, respectively. Note that the error Err_{D} of the computed solution cannot be lower than the error $\text{Err}_{\text{D},p}$ corresponding to the L^2 projected function. The following

column provides the estimated order of convergence, which in our case should be quadratic, i.e., halving the mesh parameter should result in 4 times smaller error (see [6] for details about the convergence order). In the last column we provide the number of non-preconditioned GMRES iterations needed to solve the system (2.1) with the relative accuracy $\varepsilon = 10^{-8}$.

E	N	h	$\mathrm{Err}_{\mathrm{D}}$	$\mathrm{Err}_{\mathrm{D},p}$	eoc	iter.
80	42	h_{ref}	$6.42 \cdot 10^{-1}$	$5.20 \cdot 10^{-1}$	—	11
320	162	$2^{-1} \cdot h_{\mathrm{ref}}$	$2.84 \cdot 10^{-1}$	$5.51 \cdot 10^{-2}$	2.26	17
1280	642	$2^{-2} \cdot h_{\mathrm{ref}}$	$5.31 \cdot 10^{-2}$	$1.91 \cdot 10^{-2}$	5.35	26
5120	2562	$2^{-3} \cdot h_{\mathrm{ref}}$	$9.27 \cdot 10^{-3}$	$6.85 \cdot 10^{-3}$	5.73	37
20480	10242	$2^{-4} \cdot h_{\mathrm{ref}}$	$1.94 \cdot 10^{-3}$	$1.55 \cdot 10^{-3}$	4.77	54

Table 3.1. Exterior Neumann BVP on the sphere, $\kappa = 2$.

E	N	h	$\mathrm{Err}_{\mathrm{D}}$	$\mathrm{Err}_{\mathrm{D},p}$	eoc	iter.
80	42	h_{ref}	$7.07 \cdot 10^{-1}$	$5.82 \cdot 10^{-1}$	—	14
320	162	$2^{-1} \cdot h_{\mathrm{ref}}$	$3.15 \cdot 10^{-1}$	$6.28 \cdot 10^{-2}$	2.24	20
1280	642	$2^{-2} \cdot h_{\mathrm{ref}}$	$5.91 \cdot 10^{-2}$	$2.22 \cdot 10^{-2}$	5.33	28
5120	2562	$2^{-3} \cdot h_{\mathrm{ref}}$	$1.01 \cdot 10^{-2}$	$7.49 \cdot 10^{-3}$	5.86	39
20480	10242	$2^{-4} \cdot h_{\mathrm{ref}}$	$2.13 \cdot 10^{-3}$	$1.71 \cdot 10^{-3}$	4.73	57

Table 3.2. Exterior Neumann BVP on the sphere, $\kappa = 4$.

In Figure 3.1 we present the result of the exterior Neumann BVP on a more complicated domain, namely on a simplified model of an elephant, with the testing solution $u(\boldsymbol{x}) := v_\kappa(\boldsymbol{x}, \boldsymbol{y}_2) + v_\kappa(\boldsymbol{x}, \boldsymbol{y}_3)$ with $\boldsymbol{y}_2 := [0.9, 0.25, 0.7]^\mathsf{T}$ and $\boldsymbol{y}_3 := [0.9, -0.25, 0.7]^\mathsf{T}$.

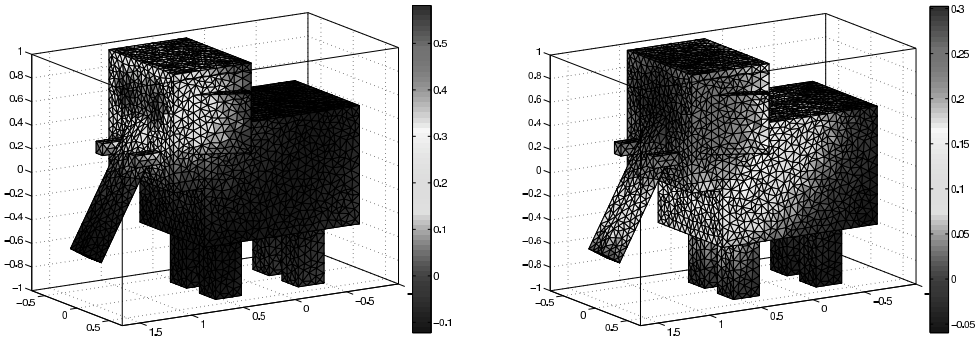

(a) Real part. (b) Imaginary part.

Figure 3.1. Solution to the exterior Neumann BVP on the elephant with $E = 7510$.

Note that in order to reach the correct convergence order on such domains, the computational mesh would have to be finer. In such a case, some BEM acceleration technique would have to be employed (see, e.g., [6] for ACA, [5] for FMM).

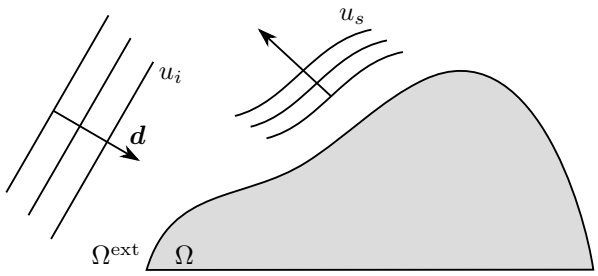

Figure 3.2. Sound scattering problem.

Let us now consider the situation depicted in Figure 3.2 with an incident sound wave $u_{\mathrm{i}} := \mathrm{e}^{\mathrm{i}\kappa\langle \boldsymbol{x}, \boldsymbol{d}\rangle}$ and the unknown scattered wave u_{s}. Assuming the so-called sound-hard scattering, the problem can be modelled by the exterior Neumann boundary value problem

$$\begin{cases} \Delta u_{\mathrm{s}} + \kappa^2 u_{\mathrm{s}} = 0 & \text{in } \Omega^{\mathrm{ext}}, \\ \dfrac{\partial u_{\mathrm{s}}}{\partial \boldsymbol{n}} = -\mathrm{i}\kappa\langle \boldsymbol{d}, \boldsymbol{n}\rangle u_{\mathrm{i}} & \text{on } \partial\Omega, \\ \Big|\Big\langle \nabla u_{\mathrm{s}}(\boldsymbol{x}), \dfrac{\boldsymbol{x}}{\|\boldsymbol{x}\|}\Big\rangle - \mathrm{i}\kappa u_{\mathrm{s}}(\boldsymbol{x})\Big| = \mathcal{O}\Big(\dfrac{1}{\|\boldsymbol{x}\|^2}\Big) & \text{for } \|\boldsymbol{x}\| \to \infty. \end{cases}$$

Note that in this case the analytic solution is not known. The computed scattered wave in the exterior of a sound-hard cube is depicted in Figure 3.3.

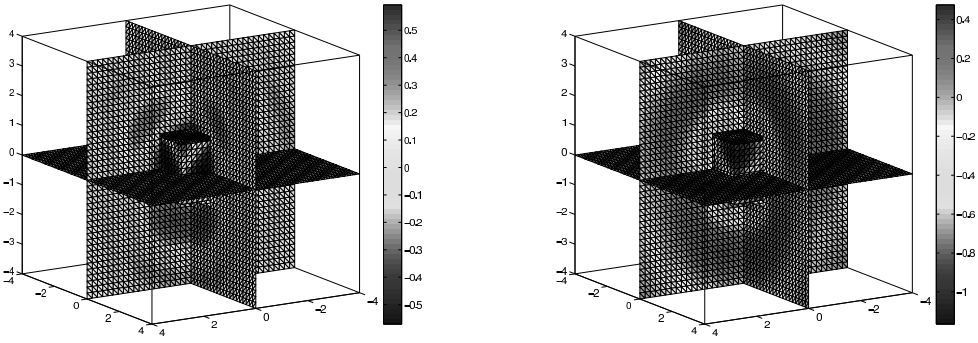

(a) Real part. (b) Imaginary part.

Figure 3.3. Scattered wave on the sound-hard cube with $E = 1200$.

More numerical experiments including Dirichlet and mixed boundary value problems for the Helmholtz equation can be found in [8].

4. Conclusion

In the paper we presented a semi-analytic calculation of the double surface integral corresponding to the hypersingular operator for the Helmholtz equation in 3D. Since the inner integral is computed analytically, it is possible to treat the singularities and compute the outer integral numerically. Numerical experiments show that the numerical error decreases at least quadratically (in agreement with the theory in [6]) and is proportional to the error of the L^2 projected exact solution.

References

[1] *R. D. Grigorieff, I. H. Sloan*: Galerkin approximation with quadrature for the screen problem in $\mathbb{R}^3$. J. Integral Equations Appl. *9* (1997), 293–319.

[2] *D. Mauersberger, I. H. Sloan*: A simplified approach to the semi-discrete Galerkin method for the single-layer equation for a plate. Mathematical Aspects of Boundary Element Methods (M. Bonnet, et al., ed.). Minisymposium during the IABEM 98 conference, France, 1998, Chapman Hall, Boca Raton. Notes Math. 414, 2000, pp. 178–190.

[3] *W. McLean*: Strongly Elliptic Systems and Boundary Integral Equations. Cambridge University Press, Cambridge, 2000.

[4] *J.-C. Nédélec*: Acoustic and Electromagnetic Equations. Integral Representations for Harmonic Problems. Applied Mathematical Sciences 144, Springer, New York, 2001.

[5] *G. Of, O. Steinbach, W. L. Wendland*: The fast multipole method for the symmetric boundary integral formulation. IMA J. Numer. Anal. *26* (2006), 272–296.

[6] *S. Rjasanow, O. Steinbach*: The Fast Solution of Boundary Integral Equations. Mathematical and Analytical Techniques with Applications to Engineering, Springer, New York, 2007.

[7] *S. Sauter, C. Schwab*: Boundary Element Methods. Springer Series in Computational Mathematics 39, Springer, Berlin, 2011.

[8] *J. Zapletal*: The Boundary Element Method for the Helmholtz Equation in 3D. MSc. thesis, Department of Applied Mathematics, VŠB-TU, Ostrava, 2011.

Authors' address: *Jan Zapletal*, *Jiří Bouchala*, Department of Applied Mathematics, VŠB-TU Ostrava, 17. listopadu 15/2172, 708 33 Ostrava-Poruba, Czech Republic, e-mail: `jan.zapletal@vsb.cz`, `jiri.bouchala@vsb.cz`.